CO4-1 Structural Change of Surfactant Micelles by Ion Capturing

K. Hara, T. Yanagino, T. Miyazaki, S. Yoshioka, Y. Oba[1], N. Sato[1] and M. Sugiyama[1]

Department of Applied Quantum Physics and Nuclear Engineering, Kyushu University
[1]*Research Reactor Institute, Kyoto University*

INTRODUCTION: Surfactants show interesting properties and are also useful for various kinds of applications. Among them, the authors have been interested in and investigating their heavy-metal capturing property intending to make use of their properties for environment purification. In such an investigation, the nano-scale structural examinations of the surfactants at several conditions are well-known to be essential because the heavy-metal capturing always follows their nano-structural changes. In the present study, the authors have investigated the nano-structural change of a surfactant, sodium oleate, in heavy water before and after the floatation treatments.

EXPERIMENTS: The 30 mM heavy-water solution of sodium oleate (SO) at several pH's (adjusted by adding HCl and NaOH) were prepared and sealed into respective quartz cells, of which the small angle neutron scattering (SANS) profiles (Fig.1) were measured after having been left intact for 24 hours at room temperature. The SANS experiments were performed with a KUR-SANS system installed at Kyoto University Reactor, Kumatori, Osaka, Japan. In addition, prepared were the 30 mM SO H_2O solutions containing 5 mM copper ion, of which the pH's were adjusted at several values after the addition of the cupric ion. The SANS profiles were also measured for some of the Cu-added SO solutions at several pH's, one of which is shown as the SANS profile plotted with ✳ in Fig. 2. Besides, the SANS profiles of the Cu-added SO solutions at several pH's were measured after the 5 min floatation treatments utilizing a glass filter with 40~50 μm pore-size and an air pump with 7.8 kPa discharge pressure (the SANS profile plotted with ◇ in Fig. 2 and Fig. 3).

RESULTS: As shown in Fig. 1, the SANS profile exhibits a distinctive peak in a pH≧8 range, indicating a distinctive structure in the SO solution. Their SANS profiles show drastic changes with the addition of Cu ion to the SO solution, as shown in Fig. 2, demonstrating the emergence of the larger structure. The SANS profiles are also largely affected by the floatation treatments as shown in Fig. 3.

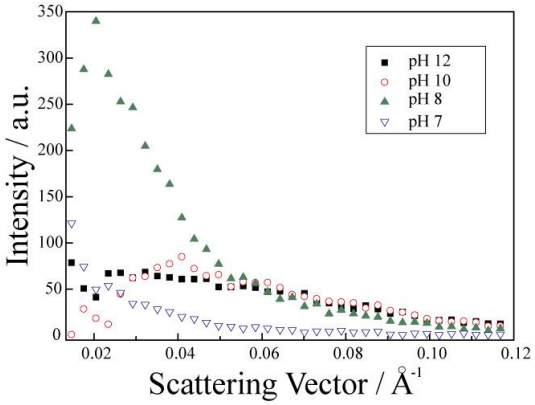

Fig. 1. The SANS profiles of 30 mM sodium oleate in heavy water at several pH's measured by KUR-SANS system.

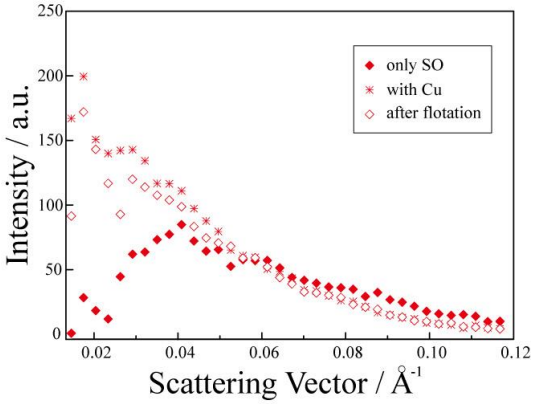

Fig. 2. The SANS profiles of 30 mM sodium oleate in heavy water: before (◆), after (✳) capturing cupper ion and after the subsequent floatation treatment at pH=10 (◇) measured by KUR-SANS system.

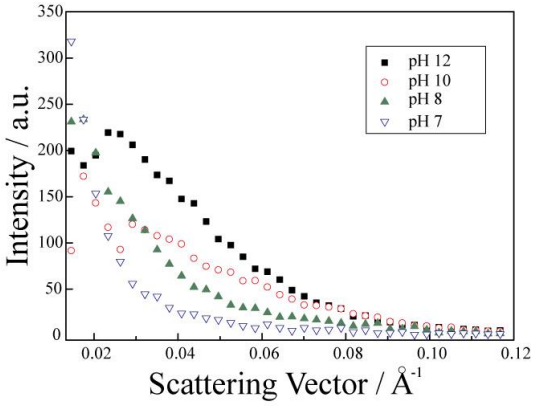

Fig. 3. The SANS profiles of 30 mM sodium oleate in heavy water after the floatation treatment at several pH's measured by KUR-SANS system.

採択課題番号 24007　界面活性剤ミセル・ゲルの重金属吸着に伴うナノ構造・ダイナミクス変化に関する研究　共同通常

(九大院・工)原　一広、柳野 智、宮崎智博、吉岡 聰　(京大・原子炉)大場洋次郎、佐藤信浩、杉山正明

CO4-2 DMSO-Assisted Grafting of Acrylamide onto PET Film by γ Irradiation

N. Rahman, N. Sato[1], S. Yoshioka, M. Sugiyama[1], K. Hara and H. Okabe

Department of Applied Quantum Physics and Nuclear Engineering, Kyushu University
[1]Research Reactor Institute, Kyoto University

INTRODUCTION: Poly(ethylene terephthalate) (PET) is a polymer which is widely used in packaging, fiber, and engineering applications due to its good mechanical strength and relatively lower production cost. Certain desirable properties such as hydrophilicity, ions adsorption can be imparted to PET film by grafting with different functional monomers. γ ray induced grafting of acrylic acid, styrene, *n*-butyl acrylate on PET films have been studied previously [1, 2, 3]. However, to the best of our knowledge, no detailed study has been reported on the γ ray induced graft copolymerization of acrylamide (AAm) onto PET films. In the present work grafting of AAm on PET film by γ irradiation was studied by using dimethyl sulfoxide (DMSO) as a swelling agent.

EXPERIMENTS: The dry PET films weighing W_{pristine} were soaked in DMSO for 0.5 h at different temperatures (from 100 to 160°C). After withdrawing the PET films from DMSO, excess liquid on the surface was removed by blotting between filter paper. The DMSO-treated PET films were taken into glass bottles containing different concentration (25, 40, 50 and 70 wt %) of AAm aqueous solutions. $FeCl_3$ at a constant concentration (1 wt %) was added after 24 h to the AAm solutions to minimize homopolymer formation. The contents of the glass bottles were then irradiated with different doses (20, 50, 70, 100 kGy) of γ rays with a dose rate of 1.0 kGy/h in air (γ-ray irradiation of the PET films was carried out at the ^{60}Co γ-ray irradiation facility of Research Reactor Institute, Kyoto University). The obtained grafted films were washed in distilled water at 60°C for 24 h to remove the homopolymers. Then the films were dried in a vacuum oven at 60°C for 24 h and were weighed ($W_{\text{AAm grafted}}$). The graft yield was determined by the percent increase in the weight as follows:

$$\delta W_{\text{AAm grafted}}(\%) = (W_{\text{AAm grafted}} - W_{\text{pristine}}) / W_{\text{pristine}} \times 100 .$$

RESULTS: When γ irradiation of pristine PET films was carried out as they were soaked in an AAm solution no grafting of AAm was observed which might be due to low diffusion of AAm solution into the polymer matrix. Therefore PET films were treated with DMSO prior to grafting, to promote the diffusion and sorption of AAm and subsequent grafting of AAm on PET by γ irradiation. Grafting of AAm onto DMSO-treated films were studied under different conditions to investigate the effects of DMSO treatment temperature, monomer concentration and total dose on graft yield which are presented in Fig. 1, Fig. 2 and Fig. 3 respectively.

REFERENCES:

[1] M. Kattan *et al.*, J. Appl. Polym. Sci., **102** (2006) 198–203.
[2] M. Nasef, J. Appl. Polym. Sci., **77** (2000) 1003–1012.
[3] X. Ping *et al.*, Radiat. Phys. Chem. **80** (2011) 632-637.

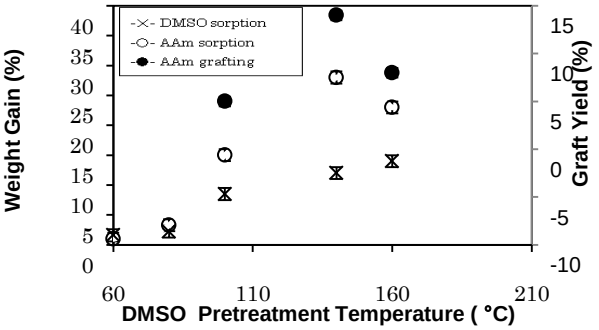

Fig. 1. Weight gain (-×- after soaking in DMSO for 0.5 h, -○- after soaking in 50 wt % AAm solution for 24 h) and graft yield (-●- for 50 wt % monomer concentration, 50 kGy dose at dose rate 1 kGy/h in presence of 1 wt % $FeCl_3$) against DMSO treatment temperature.

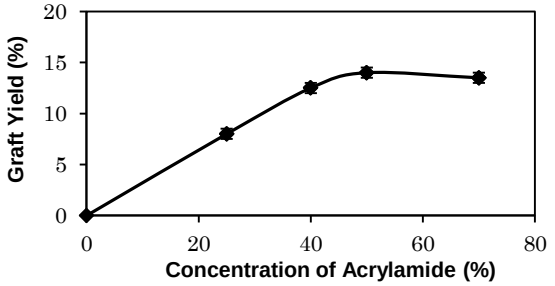

Fig. 2. Effect of monomer concentration on grafting of AAm for 140 °C DMSO treatment temperature, 50 kGy dose at dose rate 1 kGy/h in presence of 1 wt % $FeCl_3$.

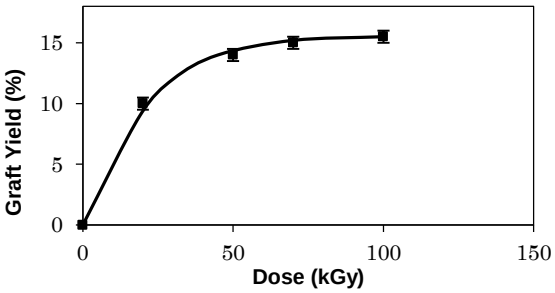

Fig. 3. Effect of dose on grafting of AAm for 140 °C DMSO treatment temperature, 50 wt % AAm concentration at dose rate 1 kGy/h in presence of 1 wt % $FeCl_3$.

採択課題番号 24010　　KUR-SANS を用いたエラストマーの中性子小角散乱観測　　共同通常
（九大院・工）Nazia Rahman、柳野 智、宮崎智博、吉岡 聰、原 一広、岡部弘高
（京大・原子炉）佐藤信浩、杉山正明

CO4-3

Mössbauer Spectroscopy of Multiferroic Iron Oxides in Applied Magnetic Field

S. Nakamura, Y. Kobayashi[1], S. Kitao[1] and M. Seto[1]

Department of Science and Engineering, Teikyo University
[1]Reserch Reactor Institute, Kyoto University

INTRODUCTION: Recently multiferroic properties of polar iron oxides have been extensively investigated. In order to clarify the mechanism of the multiferroicity, investigations using microscopic and dynamic probes are required. The ^{57}Fe Mössbauer spectroscopy is one of the appropriate probes. Especially the quadrupole splitting is very sensitive to the local environment around Fe ions and will provide useful information. Here we report the Mössbauer spectroscopy in applied magnetic field of the multiferroic oxide $CuFeO_2$.

The delafossite $CuFeO_2$ is an antiferromagnet on triangular lattice [1]. At 4.2K, the magnetic structure changes with applied magnetic field as 4-sublattice antiferromagnet (up to 7T), incommensurate proper screw spin structure (7 ~ 12T) where ferroelectricity appears (multiferroic state), and 5-sublattice antiferromagnet (above 12T) [2,3]. We have measured the corresponding Mössbauer spectra in applied magnetic field and found a change of the quadrupole splitting in the multiferroic state.

EXPERIMENTS: The single crystal of $CuFeO_2$ was provided by Dr. Noriki Terada, National Institute for Materials Science. The *c*-plane disk of 3.5mm diameter and 40μm thickness was used as an absorber. The ^{57}Fe Mössbauer spectroscopy was conducted in conventional transmission geometry by using ^{57}Co-in-Rh (50mCi) as the γ ray source. The spectra were measured at 4.2K in applied magnetic field up to 14T. The Doppler velocity was calibrated by using Fe metal foil. Lorentzian line shapes were assumed for the analysis.

RESULTS: In Fig.1, Mössbauer spectra of $CuFeO_2$ at 4.2K in applied magnetic field are shown. The quadrupole coupling constant ($e^2qQ/2$) is 0.63 mm/s under zero magnetic field. The value is three times larger than that expected from the structure, which may be due to the spin-orbit interaction. At H=5T, the spectrum is composed of two subspectra corresponding to up-moment and down-moment with intensity ratio of 1:1, which represents to the 4-sublattice antiferromagnetic state. The $e^2qQ/2$ is 0.61 mm/s and remain unchanged. At H=8T, the spectrum is composed of three subspectra corresponding to the moments with the angles of about 30°, 80°, and 160° from the H-direction. This configuration represents the incommensurate proper screw spin structure. It is noted that the $e^2qQ/2$'s are 0.57, 0.52, and 0.54 mm/s, respectively, and the all decrease noticeably in the multiferroic state. At H=14T, the spectrum is again composed of two subspectra corresponding to up-moment and down-moment with intensity ratio of 3:2, which represents the 5-sublattice antiferromagnetic state. The $e^2qQ/2$ recover to the value of 0.61 mm/s. We consider that the decrease of the $e^2qQ/2$ in the multiferroic state is related to the spin-orbit interaction .

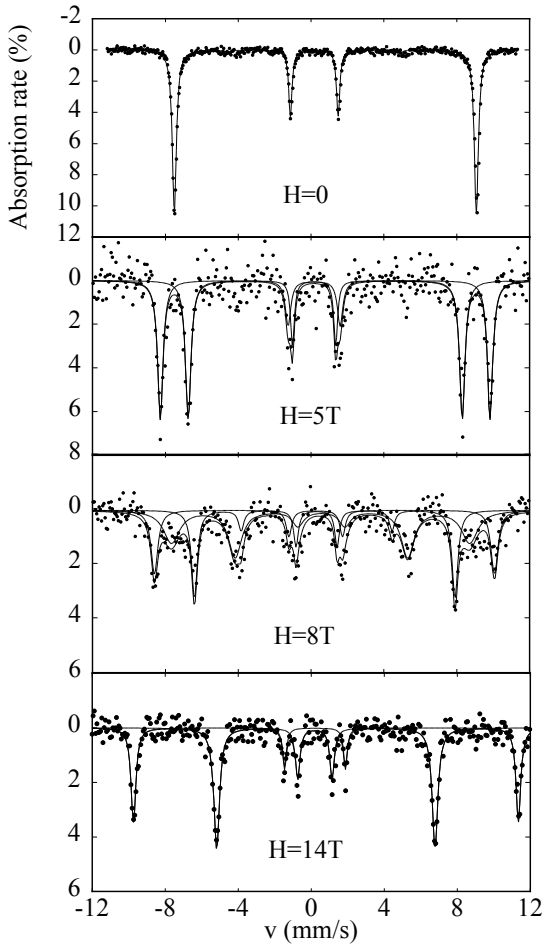

Fig. 1. Môssbauer spectra of $CuFeO_2$ at 4.2K in applied magnetic field.

REFERENCES:

[1] M. Mekata, *et al*., J. Phys. Soc. Jpn. **62** (1993) 4474.
[2] N. Terada, *et al.*, Phys. Rev. B **78** (2008) 014101.
[3] N. Terada, *et al.*, J. Phys. Soc. Jpn. **77** (2008) 054701.

採択課題番号24011　マルチフェロイック鉄酸化物の磁場中メスバウアー分光　　共同通常
（帝京大・理工）中村真一（京大・原子炉）瀬戸誠、北尾真司、小林康浩

CO4-4 Broadband Spectroscopy of Nanoporous-Gold Promoter

S. Kuwano-Nakatani, Y. H. Han , T. Takahashi[1] and T. Awano

Faculty of Engineering, Tohoku Gakuin University
[1]Research Reactor Institute, Kyoto University

INTRODUCTION: It is well known that bulk Au is inert. However, Au nanoparticles with several-nanometer-scale sizes are catalytically active for several chemical reactions such as the decomposition of formaldehyde and oxidation of CO[1]. The catalytic activity depends on the size of nanoparticles. The nanoparticles with diameters less than 3–5 nm show the highest activity for oxidation. Nanoporous Au (NPG) with 10–50 nm pore size also shows catalytic activity for oxidation.
Recently, TiO_2 is being widely used for photocatalysis of various materials. TiO_2 has a different activity with crystal structure for different wavelengths. It has been reported that composite materials of TiO_2 with Au or Pt nanoparticles enhance TiO_2 catalytic activity. TiO_2 plays an active role in the decomposition of water to generate OH radicals. It is supposed that the plasmonic electromagnetic effect of Au or Pt enhances the catalytic activity of TiO_2. In addition, since pores of NPG are able to trap the TiO_2 particles, NPG seems to be a photocatalytic nanocomposite because of enhancement of the catalytic activity by the electromagnetic effect. We have found that NPG acts as a promoter to produce OH radicals using TiO_2. We report optical properties of NPG and NPG/TiO_2 in this paper to investigate electromagnetic and plasmonic origin of the promotor effect.

EXPERIMENTS: NPG films were obtained by nitric acid etching of Ag from $Au_{35}Ag_{65}$ alloy films with about 100 nm thickness. The average pore diameter was 10–40 nm, according to the dealloying temperature and time.

RESULTS: Figure 1 shows broadband reflectivity spectra of NPG with various average pore sizes. The horizontal axis is in a logarithm to show the wide spectral range. Fine structures in IR spectra are due to CO_2 and H_2O in atmosphere. Measurement of the lack region at terahertz wave is under way at the UVSOR facility. Peaks at 0.06eV are due to reflection of the substrate quartz. It is especially strong at 42nm pore sample because of void content (low average density) of the large porous thin film. Small structures at infrared region are due to absorption by CO_2 and H_2O in atmosphere. Peaks at 1.45eV are due to reflectivity dip of the reference Al mirror. Plasmonic characteristic spectral changes were observed from IR to UV region. They depend on the pore size.

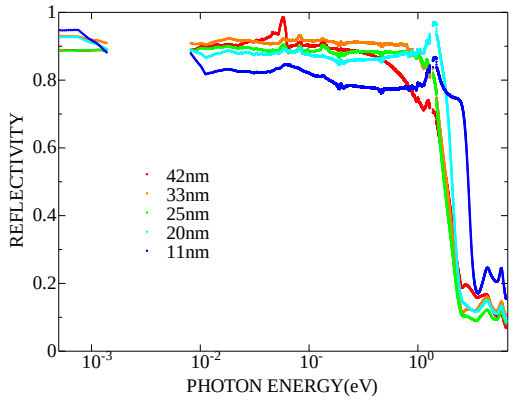

Fig. 1. Reflectivity spectra of NPG membranes on quartz substrates. Average pore diameters of the five samples with diameter on the order of 42 nm to 11 nm are shown in the NIR-UV figure.

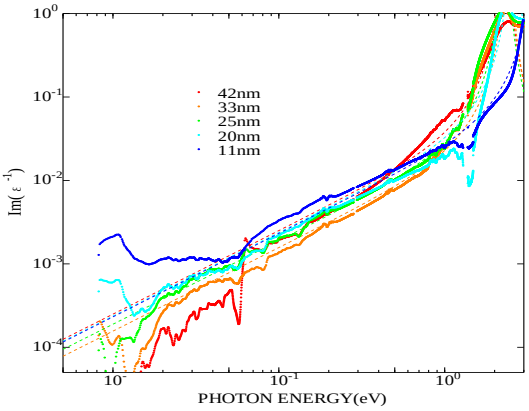

Fig. 2. Drude curve fitting of the energy loss function spectra of NPG membranes on quartz substrates. Dashed lines show fitting curves for each pore size sample.

Plasmon fitting by classical Drude model in energy loss function spectra is shown in Fig. 2. Energy loss function, Im(1/ε), is proportional to absorption intensity by transverse wave. Systematic decrease of the plasma frequency with pore size increment was observed. Plasma frequency of bulk gold is 8.6eV, therefore, these ω_p for pore samples are much small. The promoter effect seems to be related with small values of these parameters. The origin of pore size dependence of the promoter effect is still not clear.

REFERENCE:
[1] Bierner, J. *et al.*, Nature Materials, **8** (2009) 47-51.

採択課題番号 24021 超イオン導電体におけるコヒーレントミリ波誘起イオン伝導の検証 共同通常
（東北学院大・工）淡野照義
（京大・原子炉）高橋俊晴

CO4-5 Tritium Release from Li_4SiO_4 Ceramic Breeder Materials Doped with Ti

K. Munakata, K. Wada and T. Takeishi[1]
Department Faculty of Engineering and Resource Science, Akita University
[1]Graduate School of Engineering Science, Kyushu University

INTRODUCTION: The effect of titanium on the tritium release from Li_4SiO_4 ceramic breeder material was investigated. Titanium was doped in Li_4SiO_4 during the fabrication process so-called melt-spraying method. Tritium release curves were obtained in a series of experiments carried out using the out-of-pile temperature programmed desorption (TPD) technique. Tritium release curves obtained for solid breeders with different titanium composition were compared to examine the effect of catalyst metal on tritium release.

EXPERIMENTS: The titanium-doped Li_4SiO_4 ceramic breeder materials were prepared and donated by Karlsruhe Institute of Technology (KIT). These ceramic breeders with catalytic metals encapsulated in a quartz tube were irradiated in Kyoto University Research Reactor (KUR) in the thermal neutron with the flux of 5. 5×10^{12} $cm^{-2}s^{-1}$ in the He atmosphere.

Release curves of bred tritium from the breeder pebbles were obtained using the out-pile temperature programmed desorption techniques. The experimental apparatus is schematically shown by Figure 1. The volumes of ionization chambers are 66 cc and the time constant for replacement of the gas inside the chambers [volume] / [flow rate] is 40 seconds. The first ionization chamber was used to measure the total tritium concentration and the second chamber placed after a water bubbler was used to measure that of molecular form tritium in the purge gas, respectively.

Water vapor was introduced to the purge gas at the inlet of the ionization chamber when dry nitrogen gas or nitrogen with hydrogen gas was used as the purge gas to minimize the tritium memory effect according to the result obtained in the previous works.

RESULTS: Figure 2 shows comparison of experimental tritium release curves for the Li_4SiO_4 samples irradiated for 30 minutes with neutron flux with 5. 5×10^{12} $cm^{-2}s^{-1}$ [$1/cm^2s$]. The sweep gases of 1,000 ppm H_2/Ar gas were used in the experiments. Comparison of Figs. 2(a) and (b) indicates that tritium is released at lower relatively temperatures when titanium was doped to the Li_4SiO_4 breeder material. However, ionization chamber 2 was not worked. Therefore, a re-experiment needs to be conducted.

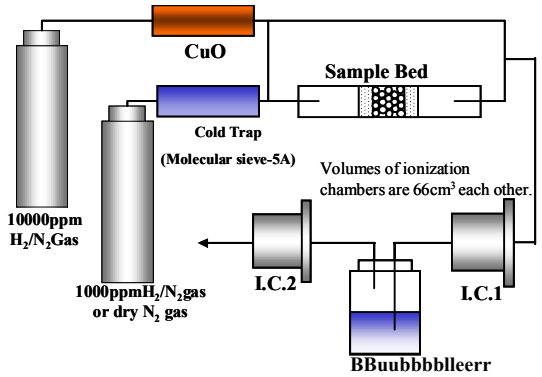

Fig.1. Schematic diagram of experimental

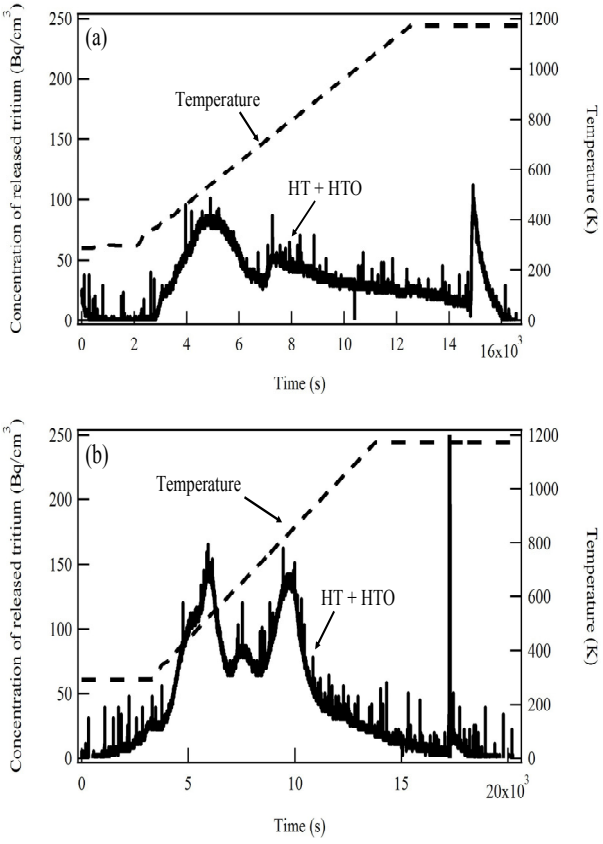

Fig. 2. Tritium release curves
(a) Li_4SiO_4 ceramic breeder material
(b) Li_4SiO_4 ceramic breeder material doped with titanium

採択課題番号　24026　　核融合炉トリチウム増殖材料および中性子増倍材料からのトリチウムの放出挙動の解明　　一般通常
（秋田大・工学資源）宗像健三、和田孝平　（九大・工学研究員）竹石敏治

CO4-6

Absorption Spectroscopy with the Coherent THz Radiation from Linac Electron Beams

S. Okuda, T. Kojima, S. Shimomura and T. Takahashi[1]

Radiation Research Center, Osaka Prefecture University
[1]Research Reactor Institute, Kyoto University

INTRODUCTION: The coherent synchrotron and transition radiation (CSR, CTR) from electron bunches of a linear accelerator (linac) have continuous spectra in a submillimeter to millimeter wavelength range at extremely high peak-intensities. The coherent radiation (CR) light sources developed were applied to absorption spectroscopy [1-4] especially for matters with relatively strong light absorbance.

The absorption spectroscopy system using the CTR from the electron beams of the 45 MeV L-band electron linac was established at KURRI [5]. The CR has high-intensity pulsed electric field and possibly excites matters in a short period. The experimental configurations have been modified for investigating such effects.

In the present work the slight changes of the transmission spectra have been observed for various kinds of matters. In order to investigate the phenomena a new pump-probe system has been developed in Osaka Prefecture University (OPU).

CHARACTERISTICS OF THE CR: The CSR is emitted as a pulsed and linearly polarized unipolar electric field. The light can produce the intense pulsed electric field and would cause the excitation in a matter. In the case of an electron linac the electric field is expected to be about 50 MV/cm. The pulse shape of the electric filed is determined by the electron bunch shape.

EXPERIMENTAL METHOD: The new experimental configurations modified for the absorption spectroscopy investigating the light intensity effects are schematically shown in Fig. 1. The output light from a light source chamber was focused at a light collimator 8 mmϕ in diameter. The spectrum of light after passing through the sample was measured with a Martin-Puplett type interferometer and a liquid-He-cooled silicon bolometer. In the previous experimental configurations the sample was located on the light path between the interferometer and the detector [5].

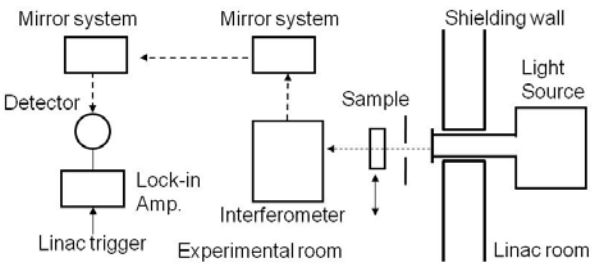

Fig. 1. Schematic diagram showing the new configurations for absorption spectroscopy using the CTR.

The spectrum was sufficiently stable during the measurements within ±2-3% in a wavenumber range of 4-12 cm^{-1}. The wavenumber resolution was 0.2 cm^{-1}. The details of the measurements are described in ref. 3.

RESULTS AND DISCUSSION: The wavenumber dependence of the transmittance of light was measured for various kinds of matters under the experimental configurations shown in Fig. 1. The change of the transmittance was observed by changing the light intensity [6]. These results seem to suggest some change in the sample induced by the pulsed CTR.

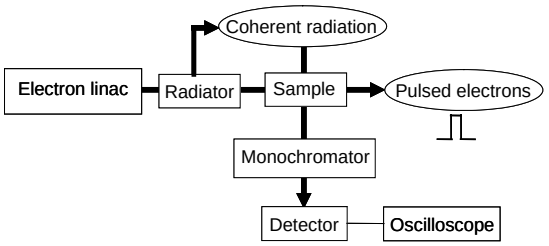

Fig. 2. Schematic diagram of the pump-probe experimental setup.

The new system for the pump-probe experiments by using the 16 MeV S-band linac in OPU has been developed [7]. Figure 2 shows schematically the components of the system, where the samples are excited with the electron beams or the pulsed CR in a short period. The CSR and the CTR is used as light sources. This will be applied to investigating the transient phenomena induced by the pulsed CR or electron beams by using CR as probe.

The light sources developed by using the electron linacs in KURRI and OPU will be applied to the excitation of matters and to the pump-probe experiments.

REFERENCES:

[1] T. Takahashi et al., Rev. Sci. Instrum. **69** (1998) 3770.
[2] K. Yokoyama, Y. Miyauchi, S. Okuda, R. Kato and T. Takahashi, Proc. 20th Int. Free-Electron Laser Conf. (1998, Williamsburg, USA) II 17-18.
[3] S. Okuda, M. Nakamura, K. Yokoyama, R. Kato and T. Takahashi, Nucl. Instrum. Meth. **A445** (2000) 267.
[4] S. Okuda et al., Radiat. Phys. Chem. **75** (2006) 903.
[5] S. Okuda and T. Takahashi, Infrared Phys. Technol. **51** (2008) 410.
[6] S. Okuda and T. Takahashi, Proc. 35th Int. Conf. on Infrared, Millimeter and Terahertz Waves (2010, Rome, Italy), IEEE Xplore 10.1109/ICIMW.2010.5612474.
[7] S. Okuda, T. Kojima, R. Taniguchi, Proc. XXV Linear Accelerator Conf. (2010, Tsukuba, Japan) 79-81.

採択課題番号24056ライナック電子線からのコヒーレントテラヘルツ放射による吸収分光 共同通常
（阪府大・地域連携）奥田修一、小嶋崇夫、下邨広元　（京大・原子炉）高橋俊晴

CO4-7 γ-Ray-Induced Preparation of Porous Binary Polymer Hydrogels

N. Sato, Y. Oba, M. Sugiyama, A. Nakamura[1] and N. Hiramatsu[1]

Research Reactor Institute, Kyoto University
[1]Faculty of Science, Fukuoka University

INTRODUCTION: Polymer gels, which are composed of crosslinked polymer chains, have network structure that provides various unique properties different from polymer solutions or polymer solids. One of them is swelling property. Polymer gels can contain large amount of liquids, especially water, inside while keeping its structure. Under favor of this property, polymer gels are widely used as a commodity material in the human life.

Polymer gels also attract scientific interests. There are many factors that characterize the structure of polymer gels: crosslink density, chemical property of component chains, electrical charge, and crosslink inhomogeneity. To obtain high quality materials using polymer gels, it is essential to reveal the relationship between structure and physical properties.

Polymer gels can be prepared through γ-ray irradiation, as well as the chemical crosslinking method. γ rays can generate reactive species directly in the irradiated materials, and thereby start the reaction without chemical additives such as reaction initiators, crosslinkers or catalysts. This advantage leads to the merit of reducing the chemical impurities in the final products, which is favorable for bio-compatible materials. In addition, less structural inhomogeneity of radiation-prepared gels than chemically-prepared gels is also advantageous for high-quality polymer gels.

The γ-ray-induced gel preparation method is also applicable to fabricate multi-component gels. Additional components can be introduced into preformed gels and firmly bonded onto existing polymer networks by radiation reaction.

In this study, we prepared two-component polymer hydrogels by the γ-ray-induced gel preparation method. Poly(ethylene glycol) (PEG) is employed as a matrix gel and poly(N-isopropylacrylamide) (PNIPAm) is introduced as a second component. PNIPAm is well known for its thermoresponsive property: swollen PNIPAm hydrogels rapidly shrink at around 34 ℃ when heated. By incorporation PNIPAm into PEG hydrogels, it can be expected that common PEG hydrogel shows such thermoresponsive behavior. Furthermore, binary porous gels can be made by γ-irradiation. Difference in structure and physical property between nonporous and porous gels was also revealed in this study.

The structural feature of nonporous and porous gels can be analyzed by several methods. Small-angle X-ray and neutron scattering analysis is useful for nm-order structure, which is discussed in another report. In this study, we are under investigating the structural difference by thermal analysis like differential scanning calorimetry. In this report, however, gel preparation and thermoresponsive behavior of these gels are described.

EXPERIMENTS: Typical preparation procedure is as follows. 10 wt% of PEG aqueous solution was sealed in a vial after removing oxygen by nitrogen bubbling. It was then irradiated with γ rays for 60 kGy at a dose rate of 1.0 kGy/h. After irradiation, the product gels were purified by removing unreacted PEG by rinsing with water several times. These PEG gels were completely dried, and then immersed in a deoxygenated 10 wt% NIPAm monomer aqueous solution. The NIPAm-impregnant gels were irradiated with γ rays again for 3.0 kGy at a dose rate of 1.0 kGy/h. After irradiation, unreacted monomers were removed by rinsing with water, and thus obtained final product gels. As for porous gels, silica microparticles (200 nm and 1000 nm) were ultrasonically dispersed in a PEG solution before irradiation and removed by hydrofluoric acid treatment after irradiation.

RESULTS AND DISCUSSION: A PEG/PNIPAm hydrogel shows no difference in appearance from pure PEG gels at temperatures lower than the transition temperature around 34 °C. When heated, however, the binary gel shrinks at around 34°C and becomes white and opaque, similarly to the PNIPAm gels. The shrunk gel is still soft and elastic although its size reduces greatly, which differs from pure PNIPAm gels. The porous gel is not dissimilar from the nonporous gel in appearance, but the change in the swelling ratio (weight ratio of the gel in the swollen state to the dried state) of the porous gel with increasing temperature is smaller than that of the nonporous gels, which means the porous gels are less shrinkable (Fig. 1). This is due to the PNIPAm chains are localized in the pore space of the PEG matrix gel. Only localized PNIAPm chains preferentially shrink in the pore, which makes the whole gel less shrinkable.

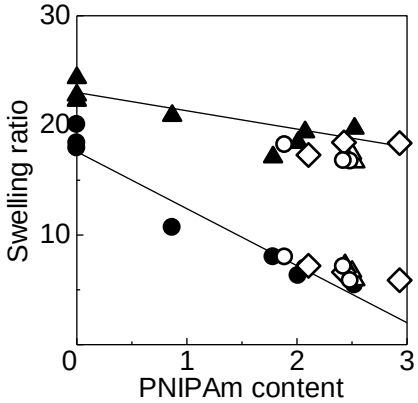

Fig. 1. Swelling behavior of porous and nonporous (open and solid symbols). Porous gels show smaller size change.

採択課題番号 24059　放射線誘起合成した多成分系高分子ゲルの熱的挙動と構造解析　　共同通常
（京大・原子炉）佐藤 信浩、杉山 正明（福岡大・理）平松 信康、中村 忠嗣

CO4-8

γ-Ray Irradiation Effects for Metal Complexes with Cage-Type Silsesquioxane Ligand

Y. Okaue, T. Yokoyama, H. Ohashi[1] and F. Yoshimura

Department of Chemistry, Faculty of Sciences, Kyushu University
[1]Faculty of Arts and Science, Kyushu University

INTRODUCTION: Upon ^{60}Co γ-ray irradiation on Q_8M_8 ($[(CH_3)_3SiO]_8(SiO_{1.5})_8$) with double four-ring (D4R) cage structure as shown in Fig. 1, hydrogen atom is stably encapsulated in D4R cage at room temperature. Encapsulation of hydrogen atom can be confirmed by ESR spectroscopy. Hydrogen atom encapsulated in D4R cage of silsesquioxane interacts magnetically with paramagnetic oxygen molecules outside D4R cage to change ESR signal intensity and saturation behavior.[1] The purpose of this study is the research for interactions between paramagnetic metal ion and encapsulated hydrogen atom in a single molecule by introducing coordination sites for metal ion to silsesquioxane with D4R cage structure. In this experiment, Schiff base site was adopted as the coordination site to form stable complexes with many metal ions easily.

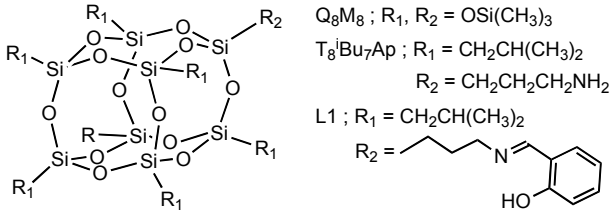

Fig. 1. D4R cage structure of silsesquioxane.

EXPERIMENTS: Ligand L1 with D4R cage structure was prepared by the reaction between $T_8{}^iBu_7Ap$ and salicylaldehyde. Various metal(II) complexes were synthesized as follows: Metal(II) acetate and L1 were stirred in methanol at 60 °C for 2-6 h. The resulting solution was concentrated under reduced pressure and cooled to room temperature. Characterizations were made by IR spectroscopy, ^{1}H NMR spectroscopy, and elemental analyses. Powder samples of metal(II) complexes were irradiated with γ-ray under air at room temperature in ^{60}Co γ-Ray Irradiation Facility at Kyoto University Research Reactor Institute. Irradiated samples were recrystallized from hexane. X-band ESR spectra for the recrystallized powder samples were measured on JEOL JES-FA200 spectrometer under air at room temperature.

RESULTS: Ligand L1 was obtained as yellow powder. The maximum yield was ca. 40%. Metal(II) complexes for Mn(II), Co(II), Ni(II), Cu(II), and Zn(II) were isolated as $M(L1)_2$. The colors and yields of the metal(II) complexes were listed in Table 1.

Table 1. Colors and yields for $M(L1)_2$

Metal	Color	Yield / %
Mn(II)	brown	70
Co(II)	light yellow	21
Ni(II)	light green	79
Cu(II)	dark green	77
Zn(II)	yellowish white	54

ESR spectra of all metal(II) complexes showed the characteristic two hyperfine lines separated with about 50 mT due to hydrogen atom nucleus (I=1/2). As an example, ESR spectrum of the irradiated $Ni(L1)_2$ was shown in Fig. 2. It was concluded that all metal(II) complexes could encapsulate hydrogen atom in the D4R cage of silsesquioxane unit. On the other hand, in the case of ESR spectrum of the irradiated $Mn(L1)_2$, the broad signal around 336 mT due to Mn(II) species was confirmed in addition to the characteristic two lines due to hydrogen atom as shown in Fig. 3.

Magnetic interactions between metal ion and encapsulated hydrogen atom in a single molecule for each complex will be examined.

REFERENCE:

[1] R. Sasamori, Y. Okaue, T. Isobe and Y. Matsuda, Science, **265** (1994) 1691-1694.

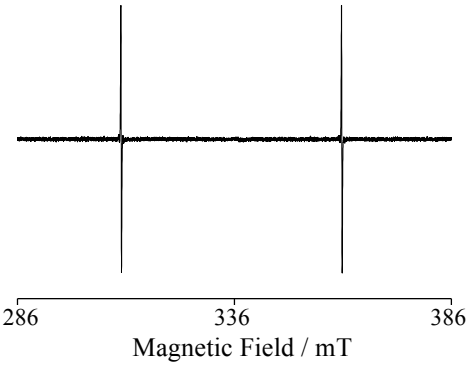

Fig. 2. ESR spectrum of irradiated $Ni(L1)_2$.

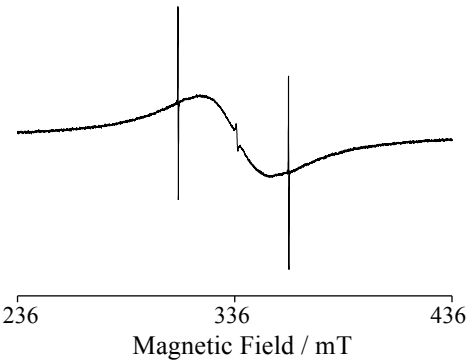

Fig. 3. ESR spectrum of irradiated $Mn(L1)_2$.

採択課題番号 24060 かご型シルセスキオキサン配位子を用いた金属錯体へのガンマ線照射効果 一般通常

（九大院・理）岡上吉広、横山拓史（九大・基幹教育院）大橋弘範（九大・理）吉村富治郎

CO4-9 Synthesis of Metal Nanoparticles Under the Gamma-ray Irradiation Field

F. Hori, K. Nagata, T. Hori, A. Okamoto, A. Iwase and M. Sakamoto[1]

Dept. of Mater. Sci., Osaka Prefecture University
[1]Research Reactor Institute, Kyoto University

INTRODUCTION: It is known that metallic nanoparticles have some specific properties, which are not appear in bulk materials such as catalytic activities, magnetic properties and so on. Also the character of them depends on its size, shape, structure, chemical composition and so on. For instance, it is known that Au nanoparticles exhibit the surface plasmon resonances (SPRs) in specific wavelength at about 520 nm. They have many possibilities to applied for various industrial fields. Generally, many kinds of metal nanoparticles commercially are synthesized by using chemical reaction method. On the other hands, it has been reported that specific feature of metallic nanoparticles can be synthesized under energetic irradiation fields, such as ultrasonic, electron, gamma-ray, plasma and so on [1-3]. Using these irradiation reduction methods, it is possible to fabricate the unexpected structured nanoparticles like a core-shell type A-B that is not appears in phase diagram [3]. In this study, we have tried to fabricate Cu nanoparticles, which is not easy to reduce in aqueous solution by chemical reaction, using gamma-ray irradiation reduction method.

EXPERIMENTS: Aqueous solutions with a given concentration of copper complex ($(CH_3COO)_2Cu \cdot H_2O$) with an additive of of sodium dodecyl sulfate (SDS) and a radical scavenger of diethylene glycol (DEG). The solution was argon purged and sealed into polystyrene vessels. They were irradiated at about 300 K with 1.17 and 1.33 MeV gamma-rays from ^{60}Co radio active source at gamma irradiation facility in KURRI, Kyoto University. The total dose was fixed to 23.4 kGy with dose rate of 15.6 kGy/h. UV–vis absorption spectra were measured by using Shimadzu UV-2550 spectrophotometer in the wavelength range in 300-800 nm and the shapes and the structures for all colloidal products were observed by conventional TEM (JEOL JEM-200CX). Samples for TEM observations were made by putting a drop of colloidal solutions on a carbon film with a Mo mesh and dried them in a vacuum.

RESULTS:
Figure 1 shows the UV/vis absorption spectra for aqueous solutions before and after gamma-ray irradiation. There is no absorption peak in aqueous solution including Cu ions before irradiation. It appears two absorption peaks around 300 and 570 nm after gamma-ray irradiation. The peak around 570 nm corresponds to the surface plasmon resonance from pure Cu nanoparticles [4]. The broadened peak around 300-400 nm may originates from the absorption of oxidic copper nanoparticles, such as CuO and Cu_2O. Therefore, both pure Cu and oxidic-Cu nanoparticles were generated in this solution by gamma-ray irradiation. TEM observation shows that generated particles by gamma-ray irradiation are monodispersive spherical shape and its average diameter is the orders of 10 nm. As a conclude that Cu nanoparticles were successfully synthesized under the gamma-ray irradiation field.

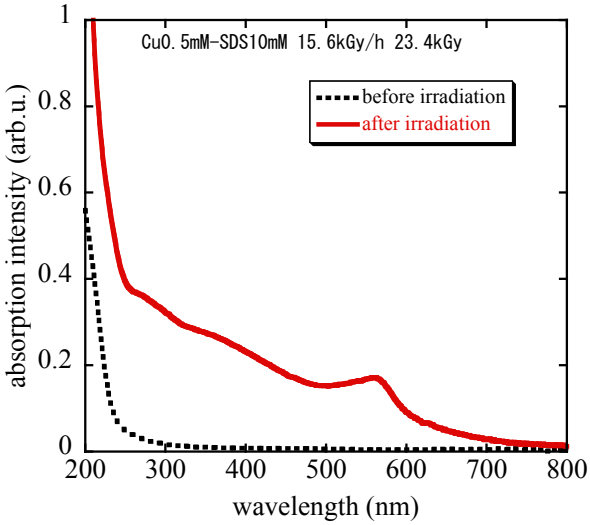

Fig. 1 UV/vis absorption spectra of aqueous solutions including Cu-ions before and after gamma-ray irradiation.

REFERENCES:

[1] T.Akita *et al.*, Catalysis Today 131 (2008) 90-97.

[2] M.Nakanishi *et al.*, Appl. Surf. Sci. 241 (2005) 209-212.

[3] N.Taguchi *et al.*, Radiation Phys. and Chem. 78 (2009) 1049-1053.

[4] Szu-Han Wu *et al.*, J. of Colloid and Interface Sci. Chem. 273 (2004) 165-169.

採択課題番号 24063 ガンマ線照射還元を利用した貴金属ナノ微粒子の創成 共同通常
（阪府大・工）堀史説、永田光一郎、堀達朗、岡本晃彦、岩瀬彰宏
（京大・原子炉）坂本雅昭

CO4-10

Magnetic Order of Fe in Normal Conducting $Sr_2VFeAsO_{3-d}$ Probed by ^{57}Fe Mössbauer Spectroscopy

Y. Tojo, T. Nakamura, M. Matoba, S. Kitao[1], M. Seto[1] and Y. Kamihara

Department of Applied Physics and Physico-Informatics, Keio University
[1]Research Reactor Institute, Kyoto University

INTRODUCTION: The discovery of high-temperature superconductivity in layered ion-based mixed anion compounds [1,2,3] represents an important breakthrough in the field of condensed matter physics. Since the discovery of the compounds, much attention has been paid to searching for new superconductors with higher superconducting transition temperature (T_c) in this family. In this study, a polycrystalline sample of $Sr_2VFeAsO_{3-d}$ as nominally d = 0.52 was prepared. The sample included minor impurity phases. The sample does not exhibit bulk superconductivity, and exhibits finite spontaneous magnetization and AF order of Fe in the sublattice at T < 15 K. These results support to obtain electronic and magnetic state phase diagram of $Sr_2VFeAsO_{3-d}$.

EXPERIMENTS: Polycrystalline samples were prepared by the solid-state reactions in a sealed silica tube using dehydrated SrO, FeAs, V_2O_5, V as starting materials, reported previously. [4] The dehydrated SrO was prepared by heating commercial $Sr(OH)_2{\cdot}8H_2O$ powder (Sigma Aldrich Japan Co. Ltd; 99.995 wt.%) at 900 °C for 10 h in air. To obtain FeAs powder, Fe (Ko-jundo Chemical Laboratory; 99.99 wt.%) and As (Ko-jundo Chemical Laboratory; 99.9999 wt.%) were mixed in a stoichiometric ratio of 1 : 1 and heated at 600 °C for 10 h in an evacuated silica tube. Then they were mixed with dehydrated SrO, V_2O_5 (Sigma Aldrich Japan Co. Ltd; 99.99 wt.%) and V (Sigma Aldrich Japan Co. Ltd; 99.9 wt.%) in the formula $Sr_2VFeAsO_{3-d}$ as nominally d= 0. The powder was pressed into the pellet shape. The pellet was loaded in an alumina tube, preventing possible reactions with the quartz tube. The alumina tube, placed in a sealed silica tube was heated to 1300 °C at a rate of 30 K/h, kept for 20 h and cooled down to room temperature. Then, the surface of the sample was polished by abrasive paper sheet made of SiC (Sankyo Rikagaku Co. Ltd; Grit no. 400 and 1000). To prevent the silica tube from collapsing during the reaction, the silica tube was filled with high purity Ar gas with a pressure of 0.2 atm at room temperature (RT). All procedures were carried out in an Ar-filled glove box (MIWA Mfg; O_2, H_2O < 1 ppm). The crystal structure, phase purity, and lattice constants of the resulting powders were examined by powder X-ray diffraction (XRD; Rigaku RINT2500 Ultra18) with CuKα radiation. DC electrical resistivity was measured by a four-probe technique using gold electrodes (Nilaco; purity 99.95 wt.%) at temperatures of 5 K to 300 K. ^{57}Fe Mössbauer spectra were obtained using conventional equipment at temperatures = 4.2-300 K.

RESULTS: Our results are summarized as follows: (i) Stoichiometric $Sr_2VFeAsO_3$ sample was not synthesized as a single phase indicating that finite oxygen deficiency is inevitable for the compound. The sample has rather large c axis than other reports. This result suggests that normal conductivity of this compound appears when the c axis is rather large. (ii) As shown in Fig. 1, the magnetic state of normal conducting sample exhibits the AF state of Fe at T < 15 K. We concluded that superconductivity does not coexist with magnetic ordered Fe sublattice. (iii) Although purer samples are required for determining the oxygen contents of $Sr_2VFeAsO_{3-d}$, our results should help in making the electronic and magnetic phase diagram of $Sr2VFeAsO_{3-d}$.

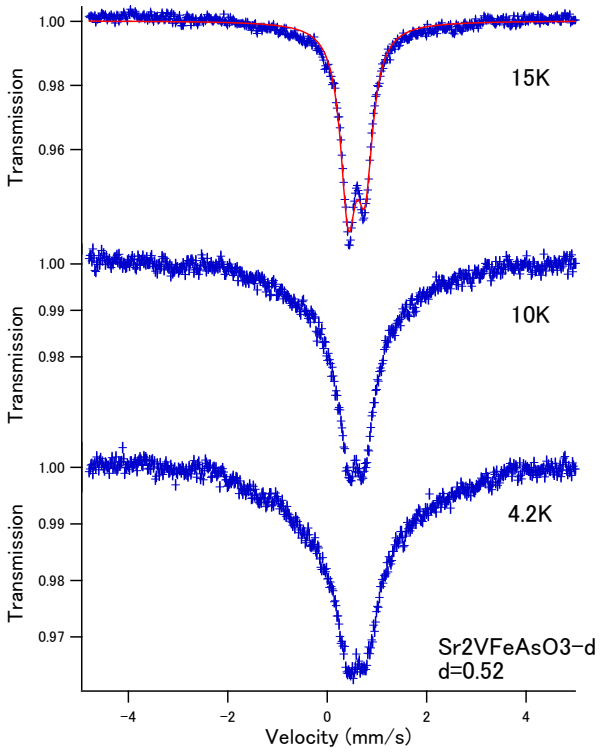

Fig. 1. ^{57}Fe Mössbauer spectra of polycrystalline $Sr_2VFeAsO_{3-d}$ at several temperatures described in the figure.

REFERENCES:

[1] Y. Kamihara, *et al.*, J. Am. Chem. Soc., **130** (2008) 3296.
[2] Y. Kamihara, Hyperfine Interact., **208** (2012) 123.
[3] X. Zhu, *et al.*, Phys. Rev. B **79** (2009) 220512.
[4] Y. Tojo, *et al.*, J. Appl. Phys., **113** (2013) 17E157.

CO4-11 Complex Structure of Ions Coordinated with Hydrophilic Polymer. 13:

A. Kawaguchi , Y. Gotoh[1] and Y. Morimoto

KURRI
[1]*Facuty of Text. Sci. and Tech., Shinshu Univ.*

INTRODUCTION: We have reported composite structure brought by *in situ* preparation through "secondary doping" by diffusion of metallic ions into iodine-doped hydrophilic polymers. Polyiodide ions, I_n^- (n = 3, 5,,), which have been doped into the polymers previously, enhances following diffusion of other molecules or ions into matrix polymer at room temperature.[1,2] As one of easier cases for diffusing operation of metallic ion, we have achieved spontaneous diffusion of silver ion (Ag^+) from $AgNO_3$(aq) into "iodine-doped polyamide-6 (PA6, Nylon^{TM}-6)". This process can develop precipitation of silver iodide (AgI) as inorganic salt at inner space of polymeric matrix and consequently provides hybrid composite for unlimited shape or size without plasticizing matrix.[3-5]
And, considering high affinity between polyiodide ions and other hydrophilic polymers (for example, PVA, starch,,), such injection procedures of inorganic ions can be applied widely for various materials; processing for hybridization can be achieved *a posteriori* for polymeric materials after their forming or structuring, so the process for hybrid composite can be applied as matrix for fiber, films, oriented structures, biological structures, textiles, micro beads and more products with arbitrary shapes and size.[5] As a case of such wide application, doping process with polyiodide was preliminarily applied for foam structure of polyurethane (PU).
EXPERIMENTS: Several kinds of commercial products "Kurara-foam"^{TM} (provided by Kurabo co.ltd.) were used as non-doped PU matrixes; all samples are soft urethane-form and are made from (poly)ester as soft segments. (In following preliminary experiments, details of the samples or their accurate components were not presented by the provider.) Pieces of PU foams were immersed into KI-I_2(aq)/0.4N. (iodine-doping) Next, these iodine-doped PU forms were immersed into $AgNO_3$(aq)/1M. (secondary doping of Ag^+) Some samples were observed with scanning electron microscopy (SEM) or wide-angle X-ray diffraction (WAXD).
RESULTS AND DISCUSSION: Generally, PU is polymer composed with two components: hard segment or hard domain containing urethane group (-NH-CO-NH-) and soft segments or soft domain composed by polyester (or polyether) binding the hard segments. PU shows low crystallinity and often amorphous induced by flexible segments.[6] On the other hand, considering polarization given by the urethane group, effects on interaction with polyiodide ions in hard segment can be expected for similarity as polyamide (PA), which often indicates ordered structures by intercalation or phase transition induced by polyiodide ions or variation in following hybrid composite.[7] Even if PU is generally amorphous, hybridization of porous foam should introduce some novel functionalities since general hybrid composites can be hardly formed as porous structure.
Consequently, iodine-doping to PU foam samples could be achieved easily at R.T. However, while diffusion of iodine advanced spontaneously from KI-I_2(aq), release (volatilization) of iodine was also activated from the iodine-doped PU and translation of polyiodide should be also in the polymer. Then, contents or components of polyiodide ion were fluctuated widely and effective data were not got for quantitative discussion at present. Generally speaking, under plenty of diffusion and release of iodine, some tendency was observed as softening the PU matrix induced by iodine-doping.
Therefore, it may be too early to estimate results quantitatively after "secondary doping" of Ag^+ ion in PU matrixes. However, macroscopic character of each sample was widely modified as hybrid composite through "secondary doping". For example, while all original PU foams had been soft and flexible and elastic porous materials, hibrid composites given by inner-precipitation of AgI were changed in quality; some of them were changed too brittle to be stretched or others were soft but sticky. It is assumed that such variation is originated in complication of coordination of iodine with PU; polyiodide can be interacted not only with explicit polarized groups (such as urethane group in hard domain) but soft segment chain (such as polyester) between them. And larger proportion of the latter soft segment chain may result the experimental uncertainty or instability in the PU hybridization.

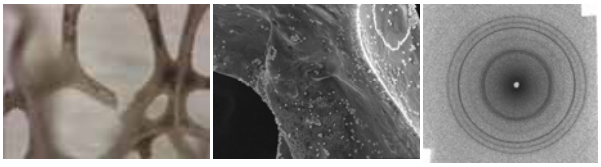

Fig. Composite with PU matrix after "secondary doping" with Ag^+; porous foam structure was modified into hybrid composite by precipitated AgI filler.

ACKNOWLEDGEMENTS: PU samples were provided by Kurabo co.ltd., The authors express great thanks for the cooperative researchers.

REFERENCES:
[1] A. Kawaguchi, Sens. Actuators B, **73** (2001) 174-178.
[2] Y. Gotoh, *et.al.*, Polym. Prep. Jpn., **51** (2002), 2259-2259.
[3] A. Kawaguchi, *et.al.*, ibid., **53** (2004), 3372-3372.
[4] A. Kawaguchi, *et.al.*, ibid., **56** (2007), 5471-5472.
[5] patent applied.
[6] "Fundamentals and Applications in Polyurethanes." (in Japanese), Ed. K. Matsunaga, (2006, CMC Press., Tokyo).
[7] A. Kawaguchi, *et.al.*, Polym. Prep. Jpn., **53** (2004), 3737-3738.

採択課題番号24079 親水性高分子ー金属塩ナノコンポジットの調製と構造 共同通常
（京大・原子炉）川口昭夫、森本幸生（信州大・繊維）後藤康夫

CO4-12 Design and Preparation of the Electrochemical Cell for the Study of the Ion Distribution at the Electrochemical Interfaces of Ionic Liquids Using Neutron Reflectometry

N. Nishi, J. Uchiyashiki and M. Hino[1]

Graduate School of Engineering, Kyoto University
[1]Research Reactor Institute, Kyoto University

INTRODUCTION: Ionic liquids (ILs), which are liquid salts entirely composed of cations and anions, have potential applications to electrochemical devices because of their several characteristics such as negligible volatility and wide potential window at the IL/electrode interface. The knowledge of the molecular-level structure at IL/electrode interface is important to optimize the performance of the IL electrochemical devices. Theoretical studies have revealed several unique features of the distribution of ions at IL/electrode interface, such as overscreening effect and lattice-saturation effect [1], while experimental studies that shed light on such features are limited to a few. In this study, we aimed to investigate the distribution of ions at the IL/electrode interface using neutron reflectometry. In this report, we will show the results of the design and the preparation of electrode film, which is crucial to sensitively detect the ion distribution.

EXPERIMENTS: Thin-layer Al_4Ti electrode film was prepared on a silicon wafer using a sputter apparatus. For IL, trioctylmethylammonium bis(nonafluorobutanesulfonyl)amide ($[TOMA^+]$ $[C_4C_4N^-]$) was prepared from the hydrophilic salts of the IL-constituent ions ($[TOMA^+]Cl^-$ and $Li^+[C_4C_4N^-]$) and purified using column chromatography. Cyclic voltammograms at the $[TOMA^+][C_4C_4N^-]$/film interface were recorded for the two-electrode electrochemical cell.

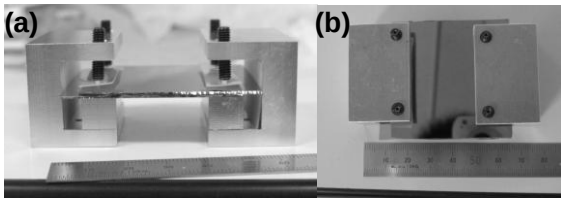

Fig. 1. (a) Side view and (b) top view of the electrochemical cell for neutron reflectivity measurements.

RESULTS: Figure 1 shows the electrochemical cell designed and prepared for neutron reflectometry. IL, $[TOMA^+][C_4C_4N^-]$, was sandwiched with two Al_4Ti electrode films that were sputtered on the surface of silicon wafers. The surface of one of the silicon wafers was polished and the surface roughness evaluated using x-ray reflectometry was ~3 Å. The interface between $[TOMA^+][C_4C_4N^-]$ and the Al_4Ti electrode film on this polished silicon surface will be "target" interface in neutron reflectometry. The surface of the other silicon wafer was non-polished because we do not want to see reflected beam from this surface and thus want to minimize and neglect the reflectivity from this surface. To prevent short circuit of the cell due to unintended contact of the two electrodes, thin layer glass sheet with a thickness of 50 μm was inserted as a spacer between the two electrodes. The area of the electrode was 30×50 mm^2 in order to keep the sufficient area to cover a long footprint of neutron beam with a grazing incident angle.

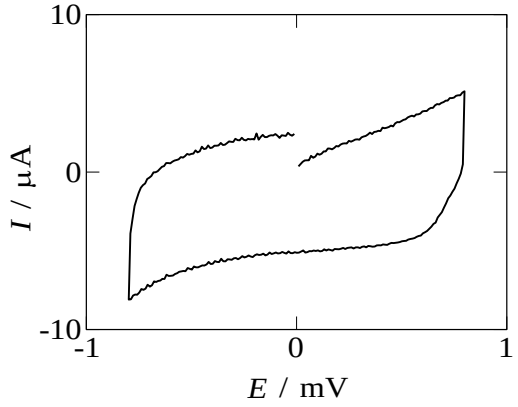

Fig. 2. Cyclic voltammogram for the electrochemical cell shown in Fig.1. Scan rate: 0.1 V s^{-1}; electrode surface area: 15 cm^2; ionic liquid layer spacing: 50 μm.

We tested the electrochemical polarizability of the $[TOMA^+][C_4C_4N^-]$/electrode interface using cyclic voltammetry. Figure 2 shows the cyclic voltammogram with a scan rate of 0.1 V s^{-1}. One can see electrochemical window with a width of 1.6 V available for the cell. The capacitance of the $[TOMA^+][C_4C_4N^-]$/electrode interface was estimated from the capacitive current recorded in the cyclic voltammogram. The capacitance was evaluated to be 3 μF cm^{-2}, lower than ~10 μF cm^{-2}, a reported value for the interface between metal and another kind of IL with smaller ions [1]. This lowering is presumably due to larger ions for $[TOMA^+][C_4C_4N^-]$ than those for the IL in ref. 1 or oxide layer formed at the surface of the Al_4Ti film.

REFERENCES:

[1] B. Roling, M. Drüschler, B. Huber, *Faraday Discuss.*, 154 (2012) 303.

採択課題番号 24082　　イオン液体｜固体界面におけるイオン多層構造の中性子反射率測定による研究　　共同通常

（京大院・工）西　直哉、内屋敷純也（京大・原子炉）日野正裕

CO4-13

Irradiation Effect on Tritum Migration Process in Tritium Breeding Material for Fusion Reactor

K. Okuno, Y. Oya, M. Kobayashi, K. Kawasaki
T. Fujishima, Y. Miyahara, H. Uchimura, T. Taguchi
K. Toda, R. Miura, T. Fujii[1], and H. Yamana[1]

Radioscience Research Laboratory, Faculty of Science, Shizuoka University
[1]Research Reactor Institute, Kyoto University

INTRODUCTION: Many studies have been carried out to establish a tritium recovery system in fusion reactors. Especially, many researchers focus on lithium titanate (Li_2TiO_3) because it is one of the candidates as the tritium breeding material for ITER due to its good tritium recovery efficiency and chemical stability. It is necessary to clarify tritium behavior from the viewpoint of fuel cycle in neutron-irradiated Li_2TiO_3. Recently, the use of $Li_{2+x}TiO_3$ (x=0.2, 0.4), which is the lithium-enriched Li_2TiO_3, is proposed to improve the tritium breeding ratio. Hara et al., reported that both of $Li_{2.2}TiO_3$ and $Li_{2.4}TiO_3$ were the mixture of Li_2TiO_3 and Li_4TiO_4, indicating that excess lithium induced the formation of Li_4TiO_4 structure in Li_2TiO_3 structure during fabrication [1]. In this study, tritium was generated in Li_4TiO_4 by thermal neutron irradiation or introduced by thermal tritium gas absorption. tritium release behavior for Li_4TiO_4 was studied by means of Thermal Desorption Spectroscopy (TDS). The tritium release kinetics for $Li_{2+x}TiO_3$ with thermal neutron irradiation were also evaluated for comparison.

EXPERIMENTAL: Powders of Li_4TiO_4 and $Li_{2+x}TiO_3$ purchased from Kaken Co. were used as samples. These were irradiated by thermal neutron with the fluence of 3.3 x 10^{15} n cm^{-2} at the Kyoto University Research Reactor Institute (KURRI). Out-of-pile tritium release experiments were performed in tritium-TDS system at Shizuoka University. In TDS experiments, the samples were heated up to 1273 K. FT-IR (Fourier Transform Infrared Spectroscopy) measurements were also carried out for Li_4TiO_4 exposed to pure D_2 gas to reveal chemical states of deuterium in Li_4TiO_4. Changes of crystal structure of Li_4TiO_4 by D_2 gas exposure were also investigated by X-ray diffraction technique at Toyama University.

RESULTS: Tritium-TDS spectrum with the heating rate of 5 K min^{-1} for $Li_{2+x}TiO_3$ with thermal neutron irradiation were consisted of two release stages at 480 K and 580 K, namely Peak 1 and 2, respectively. The activation energy of Peak 1 was estimated to be around 0.37 eV, although that of Peak 2, about 0.63 eV, corresponding to the activation energy of tritium diffusion in Li_2TiO_3[2]. Fig. 1 shows the tritium-TDS spectrum for Li_4TiO_4 with thermal neutron irradiation measured under the heating rate of 0.5 K min^{-1}. Two tritium release stages named as Peaks A and B were observed at 450 K and 600 K, respectively. As the release temperature regions of Peak 1 and Peak A were almost the same, tritium releases of these peaks were considered to be originated from the same process. In addition, it was found that O-D bonds were formed in Li_4TiO_4 by D_2 gas exposure by FT-IR measurements. On the other hand, diffraction patterns of Li_4TiO_4 with D_2 gas exposure were quite similar to that without D_2 gas exposure, indicating that LiOD structure (crystal) was not formed in Li_4TiO_4. It was reported that Li_4TiO_4 is reactive with water vapor and forms O-H bonds on the surface[1], considering that water vapor as impurity was adsorbed on the surface of Li_4TiO_4 during air exposure or TDS measurements, which would induce the formation of O-H bonds. Therefore, overall tritium release for Li_4TiO_4 was governed by decomposition of O-T bonds and appeared as Peak B in TDS spectra.

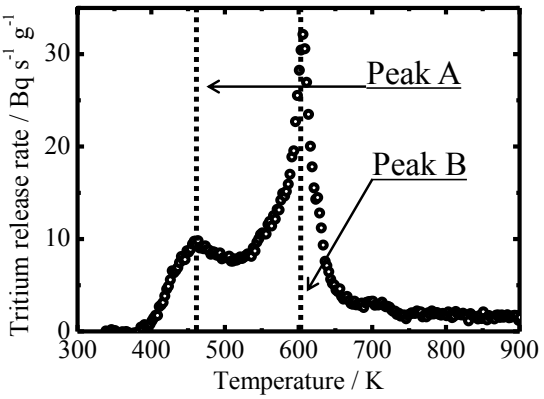

Fig. 1. Tritium-TDS spectrum of Li_4TiO_4 with thermal neutron irradiation

REFERENCES:

[1] M. Hara *et al*., J. Nucl. Mater. **404** (2010) 217.
[2] M. Kobayashi *et al*., Fusion Eng. Des. **87** (2012) 471.

採択課題番号 24083　核融合炉トリチウム増殖材中トリチウムの移行過程に及ぼす照射効果　共同通常
（静岡大・理・放射研）奥野 健二、大矢 恭久、小林 真、川崎 淨貴、藤島 徹生、宮原 祐人
内村 大道、田口 僚久、戸田 健介、三浦 遼
（京大・原子炉）山名 元、藤井 俊行、上原 章寛、中野 幸廣

CO4-14

Absorption Spectrum of Water in the Terahertz Region Using a Near-Field Aperture Probe

T. Takahashi, and S. Kimura [1, 2]

Research Reactor Institute, Kyoto University
[1]UVSOR Facility, Institute for Molecular Science
[2]School of Physical Sciences, The Graduate University for Advanced Studies

INTRODUCTION: The basic properties of the technique of near-field THz-wave microscopy has been experimentally investigated by our group [1-3]. This technique is a characteristic application of coherent radiation emitted from a relativistic electron beam, and provides high spatial resolution below the diffraction limit. In the previous report absorption spectra of cancer tissues were observed at around 11 cm^{-1} [4]. In order to investigate the origin of the absorption we have measured absorption spectra of pure water using a near-field aperture probe with coherent transition radiation (CTR) in this report.

EXPERIMENTAL PROCEDURES: The experiment was performed at the coherent radiation beamline [5] at the 40-MeV L-band linac of the Research Reactor Institute, Kyoto University. The width of the macro pulse and the repetition rate of the electron beam were 47 ns and 46 Hz, respectively. The charge of a bunch was 1.2 nC. The THz-wave source was CTR emitted from an aluminum foil with a thickness of 15-μm. The thickness of a sheet of paper tissue soaked in water was 50 μm and was put between two sheets of polyvinylidene chloride film 11 μm thick as shown in Fig. 1. The size of the aperture of the scanning probe was 775 μm. The spectra of CTR were measured by a Martin - Puplett type interferometer.

RESULTS: The observed spectra with the aperture probe were shown in Fig. 2. The absorption can be seen at around 10 cm^{-1} in the spectra both of Kimwipes and tissue soaked in water. This absorption band to date has not been known in the THz spectroscopy. On the other hand, the spectra without the aperture probe were shown in Fig. 3. The absorption band has not been observed. The size of THz wave was 10 mm on the sample. Therefore, the absorption strength at around 10 cm^{-1} depends on the irradiation size of THz wave. In order to investigate the origin of the absorption, the theoretical examination of the molecular dinamics in water is necessary.

ACKNOWLEDGMENTS: This work was partly supported by Quantum Beam Technology Program of MEXT, Japan.

REFERENCES:

[1] T. Takahashi, *et al.*, KURRI-PR 2008 CO4-10.
[2] T. Takahashi, *et al.*, KURRI-PR 2009 CO4-8.
[3] T. Takahashi, *et al.*, KURRI-PR 2010 CO4-7.
[4] T. Takahashi, *et al.*, KURRI-PR 2011 CO4-7
[5] T. Takahashi, *et al.*, Rev. Sci. Instrum. **69** (1998) 3770.

Fig.1 The photograph of the sample. The paper tissue soaked in water was put between two sheets of polyvinylidene chloride film.

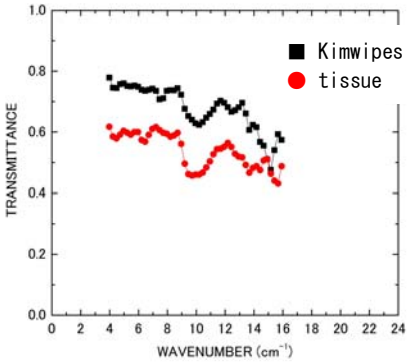

Fig.2 Observed absorption spectra of transmitted THz wave with the aperture probe.

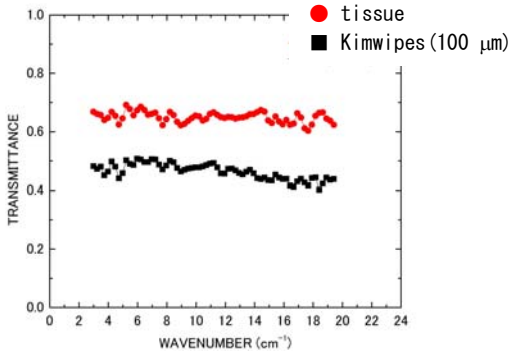

Fig.3 Observed absorption spectra of transmitted THz wave without the aperture probe. The size of THz wave on the sample was 10 mm.

採択課題番号 24084　コヒーレント遷移放射を用いたミリ波近接場イメージング分光法に関する研究　　共同通常

（分子研）木村真一（京大・原子炉）高橋俊晴

CO4-15

Property of Coherent Transition Radiation Emitted from a Pair of Wire-Grid Radiators

T. Takahashi

Research Reactor Institute, Kyoto University

INTRODUCTION: For the spectroscopic purpose, various types of coherent radiation emitted from a relativistic electron beam have attracted a considerable attention as a new and powerful light source in the THz-wave region. Coherent transition radiation (CTR) is one of such a light source. Whereas synchrotron radiation has linear polarization along an electron orbit, the electric vector of transition radiation (TR) emitted from a metallic screen is axially symmetric with respect to the trajectory of an electron beam. Therefore, CTR is usually utilized as a non-polarized light source in the spectroscopic application. However, circularly polarized light has been useful in the circular dichroism spectroscopy. Shibata *et al*. has developed a technique of generation of circularly polarized THz-wave radiation with the phase difference between the forward TR and the backward TR [1]. However, it was difficult to control the polarization degree because the geometrical arrangement was important in order to generate both the linearly polarized the forward and the backward TR. In the previous report [2] the property of the linearly polarized CTR with a radiator of a wire grid was experimentally investigated in order to develop a new technique of generation of circular polarized THz radiation. In this report a pair of wire-grid radiators with the different polarization has been used in order to eliminate the effect of the emission length.

EXPERIMENTAL PROCEDURES: The experiment was performed at the coherent radiation beamline [3] at the 40-MeV L-band linac of the Research Reactor Institute, Kyoto University. The width of the macro pulse and the repetition rate of the electron beam were 33 ns and 60 Hz, respectively. The average current of the electron beam was 3 μA. As the radiator of forward and backward CTR, wire-grid polarizers 10 μm thick with 25 μm spacing were used, respectively. The direction of grid of the first polarizer was horizontal and that of the second one was vertical. The spectrum of CTR was measured by the Martin-Puplett type interferometer.

RESULTS: The observed spectra, which were measured as varying the distance between the forward and backward radiators, are shown in Fig.1. The distance is usually called the emission length. The observed spectra are similar regardless of the emission length. Figure 2 shows the dependence of intensity on the emission length at some wavelengths in fig.1. When the emission length is far shorter than the formation length, the intensity of CTR emitted from the metallic foil is proportional to the square of the emission length [4]. Here, the formation length in the millimeter-wave region is longer than 15 m for the 40-MeV electron beam. It became clear that the CTR with horizontal polarization emitted from the forward grid is not reflected to the spectrometer by the second vertical grid and the observed intensity depends on the distance between the forward Ti window and the second grid.

REFERENCES:

[1] Y. Shibata *et al.*, Rev. Sci. Instrum. **72** (2001) 3221.

[2] T. Takahashi, *et al.*, KURRI-PR 2009 CO4-5.

[3] T. Takahashi *et al.*, Rev. Sci. Instrum. **69** (1998) 3770.

[4] Y. Shibata *et al.*, Phys. Rev. E **49** (1994) 785.

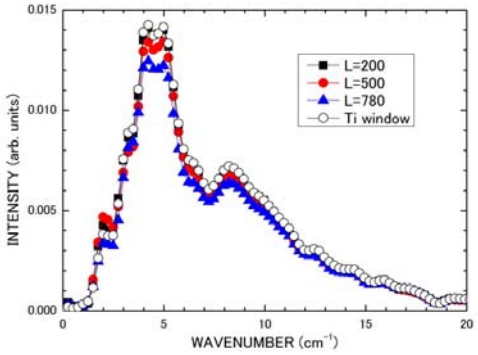

Fig.1. The observed spectra as varying the emission length (L).

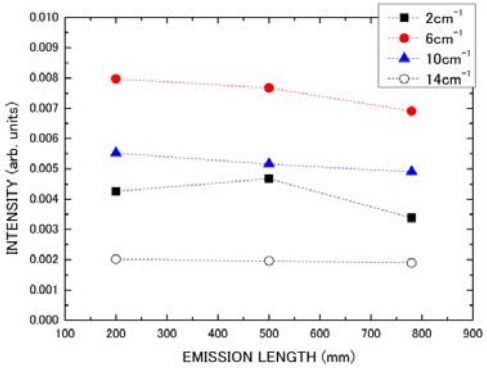

Fig.2. The relation between the observed intensity and the emission length at each wavenumber in fig.1.

採択課題番号24085　　コヒーレント遷移放射を用いたミリ波領域高時間分解分光法と円偏光の制御に関する研究　　共同通常

（京大・原子炉）高橋俊晴、窪田卓見

CO4-16 Charaterizations of Dynamic Behavior for Organic Solar Cells under High-Energry Secondary Electrons by ^{60}Co Beams

M. Oita, K Nakata[1] and Y. Sakurai[2]

Graduate School of Health Sciences, Okayama University
[1]Department of Applied Biological Science, Faculty of Science and Technology, Tokyo University of Science
[2]Research Reactor Institute, Kyoto University

INTRODUCTION: Solar cells have been used as power sources by many environmental circumstances, and played an important role in a wide range of scientific research and space development applications. For the application of satellites in space, understanding the tolerances and degradations of such cells by radiation in space is important issues [1-3]. In contrast, for medical applications for radiation dosimetry, Si-based semiconductor detectors are often used [4,5]. Recently, organic solar cells (OSC) have been widely developed due to low production costs and roll-to-roll manufacturing on flexible substrate compared to Si-based cells [6,7]. Furthermore, OSCs allow the evaluation of the radiation dose for medical practices such as radiation examinations and radiotherapy. However, the development and application of radiation detectors using solar cells are still investigated. In this work, the authors investigated the degradations and tolerance of OSCs compared to single-crystal Si-based solar cells (Si-SCs) under high-energy secondary electrons by ^{60}Co beams.

EXPERIMENTS: The samples used in this work are Si-SCs (#0906005B, Mimatsu Audio Corp, Japan) and OSCs. The surfaces of are coated by epoxy resin. The OSCs fabricated by TiO_2 photoelectrodes which were prepared by screen-printing a TiO_2 paste (Ti-Nanoxide T/SP, Solaronix SA) on fluorine-doped indium tin oxide/glass (FTO) substrates (Solaronix SA). The TiO_2 photoelectrodes were annealed at 200 °C for 10 min, and then at 500 °C for 30 min, resulting in anatase films. Multiple heating steps were performed to avoid cracking of the TiO_2 layer. The above TiO_2 photoelectrode was soaked in a solution of dye, and then dried under an air flow. A 50-μm-thick Himilan (R) film was used to assemble the TiO_2 electrode with a Pt-sputtered FTO electrode (the thickness of the Pt layer was 100 nm). The space between the electrodes was filled with a mixed electrolyte in acetonitrile. All of the samples were irradiated by ^{60}Co beams ranged from 50 Gy to 50 kGy at KUR ^{60}Co Gamma-ray Irradiation facility. To evaluate the degradation of the samples, conversion efficiencies and other electric characteristics were measured by a solar simulator (YSS-T150A, YAMASHITA DENSO Corp.) before and after irradiation.

RESULTS: Fig. 1 shows the degradation of conversion efficiencies for OSCs as compared to Si-SCs by radiation. There were no significant changes between OSCs and Si-SCs less than 5 kGy. Fig. 2 shows the degradations of the short-circuit current density for OSCs as compared to Si-SCs by radiation. The degradations of the output current for OSCs were observed about less than 1% / kGy. In summary, high-energy secondary electrons by ^{60}Co beams irradiated and investigated the radiation tolerance of OSCs. These results reveal that the dosimetry devices using OSCs would be feasible for medical application.

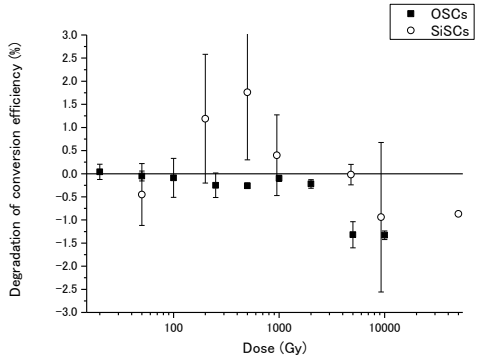

Fig. 1. The degradation of conversion efficiency for OSCs and Si-SCs under secondary electrons by ^{60}Co beams.

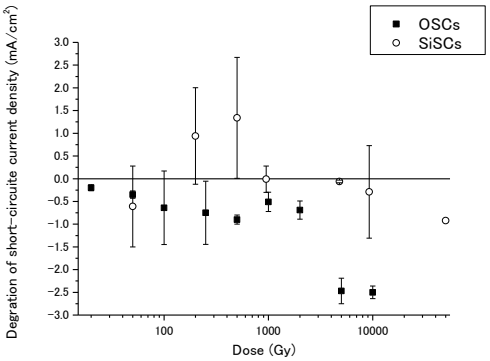

Fig. 2. Degradation of short-circuit current density for OSCs and Si-SCs under secondary electrons by ^{60}Co beams.

REFERENCES:

[1] A. Khan *et al.*, J. Appl. Phys., **87** (2000) 2162.
[2] J. Haapamaa *et al*, Solar Energy Materials & Solar Cells, **66** (2001) 573.
[3] A. Khan *et al.*, Solar Energy Materials & Solar Cells, **75** (2003) 271.
[4] Bo. Nilsson *et al.*, Radiotherapy and Oncology, **11** (1988) 279.
[5] D. Menichelli *et al.*, Nucl. Instr. and Meth. A, **583** (2007) 109.
[6] M. Manceau *et al.*, Organic Electronics, **12** (2011) 566.
[7] J-W Kang *et al.*, Solar Energy Materials & Solar Cells, **103** (20127) 76.

採択課題番号 24095 高エネルギー粒子線による有機系太陽電池の動的挙動に関する研究　共同通常
（岡山大・保）笈田将皇（東京理科大・理工）中田一弥（京大・原子炉）櫻井良憲

CO4-17 Activation Analysis of Tungsten Deposited on Graphite Tiles of JT-60U Tokamak

Y. Ueda, Y. Meichang, K. Jo[1] and M. Fukumoto[2]

Graduate School of Engineering, Osaka University
[1]Graduate School of Science, Kyoto University
[2]Japan Atomic Energy Agency

INTRODUCTION: Tungsten local transport in the JT-60U tokamak device (JAEA) has been studied. Tungsten coated CFC tiles were installed in the outer divertor position, on which outer strike points did not normally stay. Tungsten on inner divertor tiles existed in the thick carbon deposition layer (more than 100 μm in thickness), which makes estimation of total amount of tungsten deposition difficult by conventional surface analysis methods (e.g. XPS, AES). In order to measure the total amount of tungsten in the thick carbon deposition, a neutron activation method by the KUR fission reactor was employed. In the fiscal year of 2012, first trial of the activation experiments of carbon samples containing tungsten deposits was done.

EXPERIMENTS: The samples were prepared in a JAEA Naka cite. Since C deposition layers are very fragile, surfaced of the tiles were covered by sticky transparent tapes for protection. Sizes of the samples were about 10 x 10 x 1 mm. Since graphite base materials contain very few impurities, activation elements in the samples are mostly tungsten, which was confirmed by a previous neutron activation experiment [1].

Three graphite samples and one pure tungsten sample (0.5 mg) were installed in a plastic capsule, which was exposed to neutrons by 1MW KUR operation for four hours. Then it was kept for about three months to wait for cooling down of short lived tungsten isotopes (mainly ^{187}W, 23.5 hours), leaving long lived isotopes (mainly ^{185}W, 75 days). Gamma spectrum was measured by a Ge semiconductor detector.

RESULTS: Unfortunately, graphite samples with the dimensions of 10 x 10 x 1 did not have enough strength to withstand a transfer process to KUR by compressed air. They were cracked and given up for activation measurement. Fig. 1 showed gamma spectrum of the activated pure W sample. No gamma rays from ^{185}W were observed, probably because neutron exposure time was too short to make enough activation. On the other hand, radiation from a short lived isotope (^{187}W) almost disappeared in this measurement. Since total amount of tungsten deposition on W samples are similar or less than that of the pure tungsten, it turns out that this activation analysis method is not useful to tungsten deposition measurement on JT-60 tiles.

The other possibility is to use the shot lived isotope

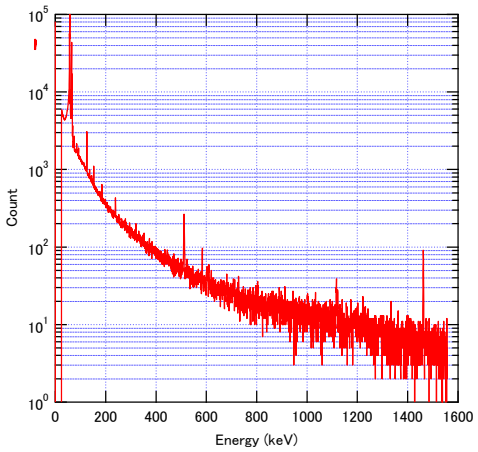

Fig.1 Gamma ray spectrum from a pure tungsten sample

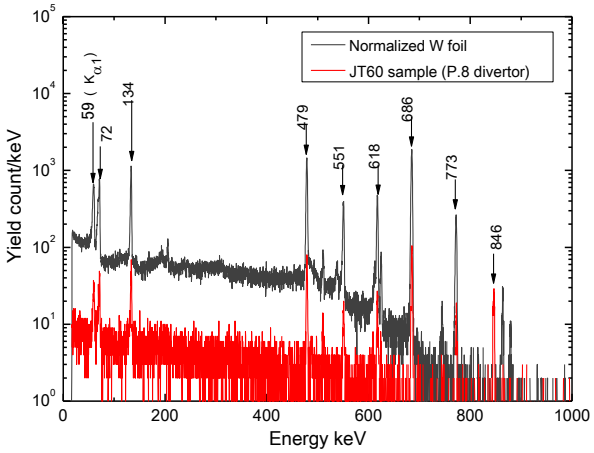

Fig. 2 Gamma ray spectrum from a neutron-activated sample by FNS. Gamma mainly from ^{187}W was detected.

(^{187}W), which will emit stronger gamma ray signal than ^{185}W. An example is shown in Fig. 2. These data were taken also by a neutron activation method previously performed at FNS in JAEA. In Fig. 2, gamma spectrum from pure W (larger signal) and that from a JT-60U sample. Several lines (e.g. 479 keV, 686 keV etc.) from ^{187}W were clearly observed in this experiment. In next experiment, we plan to use these lines to determine tungsten deposition on JT-60U samples. In addition, it is important to find more suitable sample size (probably thicker samples are better) and to insert shock absorber in a capsule to avoid breakdown of graphite samples.

REFERENCES:

[1] Y. Ueda et al., Nucl. Fusion 49 (2009) 065027 (7pp).

採択課題番号 24100　　JT-60 トカマク装置の炭素タイル上に堆積した　　共同通常
タングステンの放射化分析

（阪大・工）上田良夫、余 美昌（京大・原子炉）徐 虬（原子力機構）福本正勝

CO4-18 Ground Plane of the B–3 Beam Port of KUR

K. Mori, H. Yoshino, S. Sato[1], S. Muto[1], K. Iwase[2], S. Tomihira[3], T. Fukunaga and Y. Kawabata

Research Reactor Institute, Kyoto University (KURRI)
[1]High Energy Accelerator Research Organization (KEK)
[2]Department of Materials and Engineering, Ibaraki University
[3]Graduate School of Engineering, Kyoto University

INTRODUCTION: The B–3 beam port of Kyoto University Research Reactor (KUR) had long been used as a four-circle single-crystal neutron diffractometer (4CND). For the last decade, however, the 4CND was so old that its research activity on neutron science was quite low. Therefore, the 4CND needed to be replaced and a new neutron diffractometer has been required at the B–3 beam port. Meanwhile, the growing demand to study the atomic structure of the various kinds of materials promotes the use of neutron scattering techniques. In particular, the neutron (powder) diffraction is a powerful tool to determine the positions of light elements (e.g., hydrogen and lithium) in energy storage materials such as hydrogen absorbing materials and lithium-ion batteries.

Here, we report the ground plane of the B-3 beam port of KUR, particularly the "compact" multipurpose neutron diffractometer. In addition, we have a plane to utilize for the study of the neutron detector development by the data acquisition group of the neutron science division of KEK (KEK–KENS DAQ group) at the B-3 beam port, as we mention below.

DESIGN CONCEPT OF B–3: Figure 1 shows the schematic perspective view of the compact multipurpose neutron diffractometer. The neutron wavelength (λ), which is monochromatized by the (220) plane of a Cu single crystal, is 1 Å. To cover the detector area ($6\ ^{\circ} \leq 2\theta \leq 150\ ^{\circ}$), 36 ^{3}He tube detectors (1/2 inch diameter) will be used. The distances from the monochromator to the sample and from the sample to the detector will be 1.9 m and 1.2 m, respectively. In the second period of the neutron beam time in fiscal 2012, the preliminary neutron diffraction experiments were conducted with standard powder samples (e.g., Ni) and hydrogen absorbing alloy ones, using 6 ^{3}He tube detectors, instead of an old BF_3 detector of the 4CND. In spite of high background intensities, we succeeded to observe their several Bragg reflections, which could be indexed on the basis of $\lambda = 1$ Å.

DEVELOPMENT OF NEUTRON DETECTOR SYSTEM: The B–3 beam port has a wide space around the sample; therefore we can easily install any other system. The KEK–KENS DAQ group has used the B–3 beam port to assess their new ^{6}Li-glass neutron detector system, LiTA12, as shown in Fig. 2. The LiTA12 system consists of a ^{6}Li-glass neutron detector with a multi-anode photo multiplier tube (MA–PMT), an amplifier, and an analog-to-digital converter (ADC) board. The further investigations are now in progress.

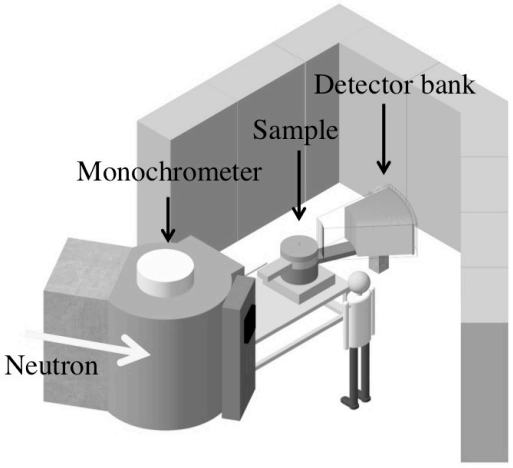

Fig. 1. The schematic perspective view of the compact multipurpose neutron diffractometer at the B–3 beam port of KUR.

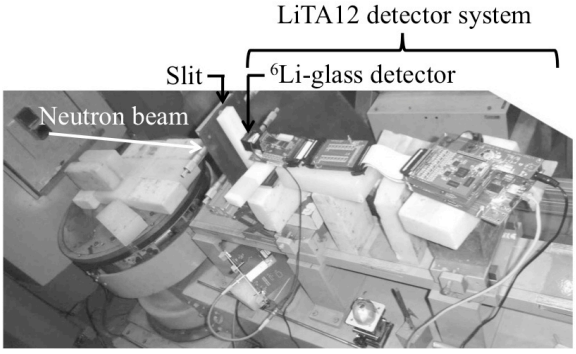

Fig. 2. New ^{6}Li-glass neutron detector system, LiTA12, which has been developed by the KEK–KENS DAQ group.

ACKNOWLEDGEMENTS: We would like to thank the KEK–KENS for providing the equipment for neutron diffraction experiments; ^{3}He tube detectors, etc. We are grateful to Ms. T. Mori for drawing the schematic illustrations of the compact multipurpose neutron diffractometer.

採択課題番号 24106　材料研究および中性子検出器開発を目的とした　　共同即時
多目的型簡易粉末回折装置の建設
（京大・原子炉）森　一広、吉野泰史、福永俊晴、川端祐司（高エネ研）佐藤節夫、武藤　豪
（茨城大・工）岩瀬謙二（京大院・工）冨平昌吾

CO4-19 Radiation Anomaly Invesitgation of Nano-Satellite “Horyu-II”

Y. Okumura, H. Masui, M. Cho and K. Takamiya[1]

Kyushu Institute of Technology
[1]Research Reactor Institute, Kyoto University

INTRODUCTION: Recently universities and venture businesses actively develop micro/nano-satellites. Horyu-II launched in May 2012 suffered anomaly by radiation. Radiation test is important to investigate the cause. Conventional radiation test needs an accelerator. The cost is too high for micro/nano-satellites. Radiation test with californium-252 will give us an affordable solution.

EXPERIMENTS: The purpose of the test is to detect SEE (Single Event Effect) using californm-252 and reproduce the anomaly phenomenon of Horyu-II. The anomaly occurred in H8 microcomputer which processed all the data of the satellite. We used a spare board of Horyu-II and irradiated 2 points shown in Fig. 1. The plastic packages were removed to make radiation particles penetrating.

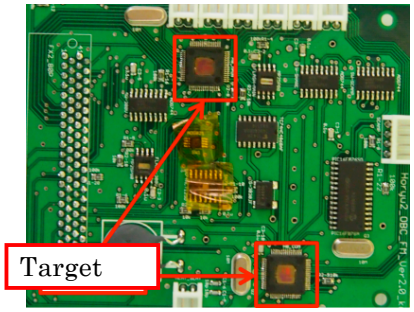

Fig. 1. Irradiation targets

The experimental schematic is illustrated in Fig. 2 (Side view of the circuit board). We monitored the current consumed by the circuit boards.
ion of OBC and all system.

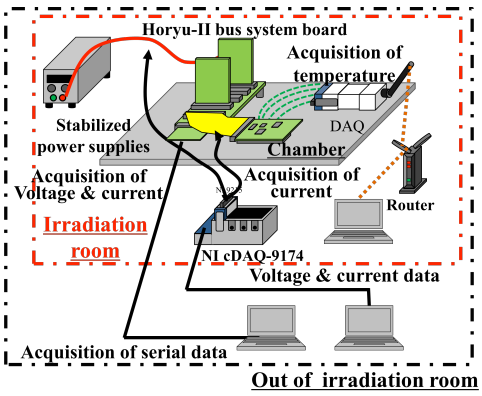

Fig. 2. Experiment schematics

RESULTS: While the targets were irradiated, we detected malfunction of the H8 processors. Fig.3 shows the current consumption of the circuit boards. First, the radiation source was placed over H8-Main that handles data processing. During the section (i), the experimental boards were working normally. The jump in the current near 250s is due to the start of the communication. In section (ii), malfunction on H8-Main occurred and at the same time, the current jumped by 0.1 A. We tried to reset H8-Main via a command, but failed. We moved the radiation source over H8-COM that handles communication. In section (iii), H8-COM malfunctioned and the current also jumped by another 0.1A.

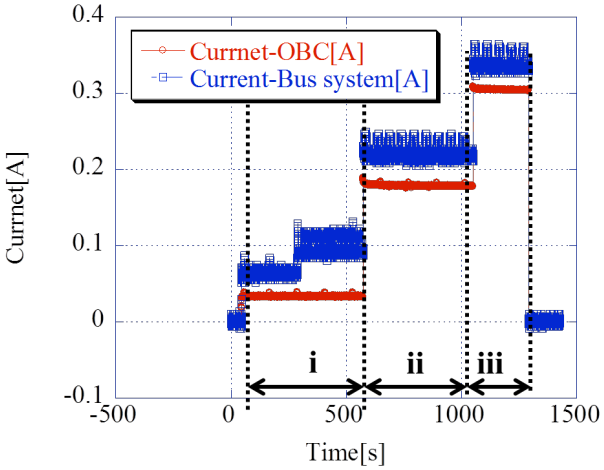

Fig. 3. Consumption current of the satellite system

Fig. 4 summarizes Horyu-II’s anomaly observed in orbit. The upper figure is Normal mode. The middle figure is the first anomaly observed. The sensor data in the downlink telemetry became frozen. This phenomenon can be explained by the malfunction of H8-Main. The bottom figure shows the second anomaly. Horyu-II couldn’t send even the frozen sensor data back. This phenomenon can be explained by the malfunction of H8-COM. Therefore, we conclude Horyu-II’s anomaly was caused by single event effect of H8 processors.

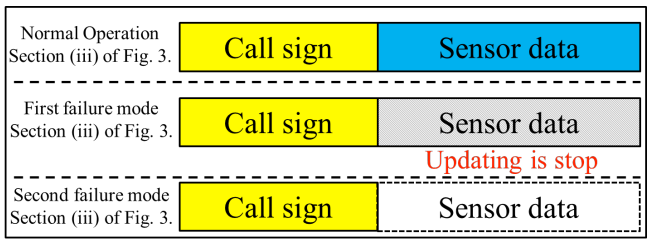

Fig. 4. Failure mode

REFERENCES:

[1] Stephen J H, Sanderson T K, Mapper D, Farren J. IEEE Trans. Nucl. Sci., 1984, NS-31(6): 106

採択課題番号24108　カリフォルニウム線源を使用した衛星搭載用オンボードコンピュータに発生する　共同即時シングルイベントの模擬試験および試験方法の確立
（九工大・先端）奥村　裕太、増井　博一、趙　孟佑（京大・原子炉）高宮　幸一